Article

Journal of
Nanoscience and Nanotechnology
Vol. 17, 3460–3464, 2017
www.aspbs.com/jnn

Electrical Properties of Sputter-Deposited InGaZnO Thin Film Transistors with an Etch Stopper

Jin-Kuk Kim[1], Seong Min Shin[1], Jinsung Choi[2], Byung Seong Bae[1], and Eui-Jung Yun[3,*]

[1] Department of Display Engineering, Hoseo University, Asan, Chungnam, 31499, South Korea
[2] Department of NanoBio Tronics, Hoseo University, Asan, Chungnam, 31499, South Korea
[3] Department of Information Communication Technology and Automotive Engineering, Hoseo University, Asan, Chungnam, 31499, South Korea

This study demonstrated the effect of a passivation layer of a siloxane-based spin-on-glass (SOG) etch stopper on the electrical properties of sputter-deposited InGaZnO thin-film transistors (IGZO TFTs). Compared to stabilities of unpassivated devices, IGZO TFTs passivated by SOG annealed at 100 °C in air showed better stability against positive bias stress (PBS) and much worse stability against negative bias stress (NBS), which were attributed to the reduction of ambient environmental effects by SOG and the introduction of H and C electron donors from SOG into IGZO. As the annealing temperature of SOG increases from 100 to 300 °C, the degradation in PBS stability and the improvement in NBS stability were observed. These are because of higher O-related acceptors and lower C- and H-related donors in IGZO, respectively, as evidenced by SIMS analysis. The best stability was achieved for the passivated TFTs with a 200 °C-annealed SOG, which exhibited a small threshold voltage shift (ΔV_{th}) of 2.1 V under PBS and a minimal ΔV_{th} of 1.8 V under NBS. These results show the great potential of methyl-siloxane-based SOG layers as effective passivation materials.

Keywords: InGaZnO Thin-Film Transistor, Etch Stopper, Sputter-Deposited.

1. INTRODUCTION

Recently, amorphous indium-gallium-zinc oxide thin-film transistors (a-IGZO TFTs) with the bottom gate structure have been widely used as a switching device for organic light-emitting diode (OLED) and flexible electronics due to their superior properties, such as higher field-effect mobility than that of amorphous silicon (Si) TFTs, good uniformity compared with polycrystalline Si TFTs, good optical transparency in visible light region, possibility of low-temperature process, and high throughput.[1–11] On the other hand, the stability of a-IGZO TFTs under the applications of constant gate bias stress has recently become a main issue in unpassivated TFTs with a bottom gate structure.[12–16] It has been reported[14–17] that the reliability of a-IGZO TFTs was degraded by ambient effects which are related to adsorption–desorption of oxygen and water molecules from ambient onto the exposed back-channel surface. Therefore, to improve the stability of a-IGZO TFTs, passivation layers have been commonly required.

Various inorganic passivation layers such as SiO_x,[18,19] Al_2O_3,[18,20] Y_2O_3,[18] TiO_2,[18] MgO,[21] SiN_x,[14] AlO_x[22] were used. However, these inorganic passivation layers are usually deposited by using more complicated and high-cost vacuum processes which induce the negative effects on the TFTs performance due to plasma damage that creates trap states at the channel-gate insulator interface.[16] An etch stopper layer, which acts as aforementioned passivation layer, was also employed to protect the channel from plasma-induced damage during dry etching of source/drain electrodes and to realize IGZO TFTs with high mobility.[23,24] Several organic passivation layers such as photoacryl,[17] paraffin wax,[25] and CYTOP[26] have been proposed because they are much easier to deposit through a simple solution process or sol–gel method compared to their organic counterparts. Moreover, photosensitive organic-inorganic hybrid passivation layers based on polysilsesquioxane[15,16] have been suggested in a-IGZO TFTs. However, organic passivation layers were frequently degraded the transfer characteristics and reliability of a-IGZO TFTs. Therefore, a variety of organic passivation

*Author to whom correspondence should be addressed.

 1533-4880/2017/17/3460/005 doi:10.1166/jnn.2017.14022

layers will need to be investigated to improve the stability for the a-IGZO TFTs. In this paper, we explored the influence of new methyl-siloxane-based organic passivation layer on the device stability against constant gate bias stresses of a-IGZO TFTs formed by a simple fabrication process which uses the shadow mask technique to pattern the channel and source/drain electrodes.

2. EXPERIMENTAL DETAILS

The a-IGZO TFTs with the SOG passivation film were fabricated on SiO_2 oxide layer thermally-grown onto a heavily-doped p-type Si substrate. A Si substrate and a 300-nm-thick SiO_2 were used as a gate electrode and a gate insulator, respectively. A 50-nm-thick a-IGZO channel layer was deposited at 200 °C using a sputter target of In:Ga:Zn = 1:1:1 in atomic ratio under the following conditions: RF power of 50 W, working pressure of 5 mtorr, and O_2 ratio of 25%. The shadow mask was used to pattern the a-IGZO channel layer. The channel layer was post-annealed at 400 °C for 1 hour in air after deposition. Subsequently, the methyl-siloxane-based SOG etch-stopper layer (ESL), which acts as a passivation layer and contains organic dopants of CH_3 or C_2H, was deposited with a sol–gel method. The SOG solution was filtered through a 0.2-μm poly-tetra-fluoro-ethylene (PTFE) filter and spin-coated at 3000 rpm for 30 s. Then, the SOG solution was converted to SiO_2 by thermal annealing at different temperatures in ranges of 100–300 °C in air for 1 hr on a hot plate to evaporate solvent. The ESL was patterned by a photolithography process using following dry etching conditions: RF power of 196 W, working pressure of 100 mtorr, and mixed gas ratio of CF_4:O_2 = 60:20. Here, we emphasize that some samples with the same structure were fabricated without the ESL to explore the effects of the passivation layer on the stability properties of the fabricated TFTs. Finally, the 150-nm-thick Al source–drain electrodes were deposited by DC magnetron sputtering and patterned by using shadow mask. An annealing of all developed TFTs was performed at 150 °C for 1 hour in air after the TFTs had been placed in a built-in heating element to make an ohmic contact between the channel and source–drain electrodes. Figure 1 shows a schematic cross-sectional view and a photographic top view of typical a-IGZO based TFTs with a siloxane-based SOG passivation layer developed in this study. As shown in Figure 1, the TFTs have the bottom gate and top contact structure. The channel width (W) and the channel length (L) were the same, 1000 μm.

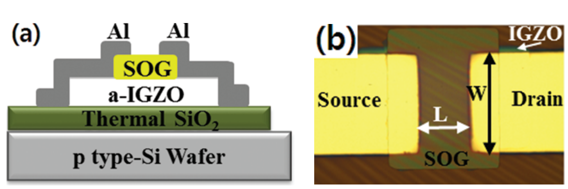

Figure 1. (a) Schematic cross-sectional view and (b) photographic top view of the a-IGZO TFTs with a siloxane-based SOG passivation layer developed in this work: $W = 1000$ μm and $L = 1000$ μm.

To investigate the changes in the depth profiles of various elements in the a-IGZO TFT structures, secondary ion mass spectroscopy (SIMS) analyses were carried out using a Cs^+ gun with following conditions: impact energy of 14.5 keV, current of 10 nA, and raster size of 130 μm. Negative-bias-stress (NBS) and positive-bias-stress (PBS) were applied at room temperature in air and the gate-to-source voltage (V_{GS}) was fixed at −20 and 20 V, respectively. During NBS and PBS, the drain and the source electrodes were grounded, and a maximum stress time of 3.6×10^3 s was used. The gate-bias stress and device characteristics of the a-IGZO-based TFTs were measured in a darkened probe box by using two Keithley 2400 source meters for a DC voltage source and a Keithley 6485 picoammeter for current measurements.

3. RESULTS AND DISCUSSION

Table I summarizes the important device parameters at two stress time (τ_{st}) values of 0 and 3600 s, which were obtained from the evolution of the drain-to-source current versus V_{GS} (I_{DS}–V_{GS}) transfer curves as a function of τ_{st} for the unpassivated a-IGZO-based TFTs under PBS with V_{GS} of 20 V and NBS with V_{GS} of −20 V. All measurements were performed with the drain-to-source voltage (V_{DS}) fixed at 10 V, which is in the saturation region. The slopes of the sub-threshold swing (SS) were obtained from the inverse slopes of the transfer curves. The saturation field-effect mobility μ_{eff} was also estimated using Eq. (1):

$$\mu_{eff} = \left(\frac{\partial\sqrt{I_{DS}}}{\partial V_{GS}}\right)^2 \frac{2L}{W}\frac{1}{C_{ox}} \quad (1)$$

where C_{ox} is the capacitance per unit area of the SiO_2 gate insulator, which was ∼11.8 nF/cm^2 as measured in a metal-insulator-metal configuration. As listed in Table I, with increasing τ_{st}, the threshold voltage (V_{th}) was shifted positively ($\Delta V_{th\text{-PBS}} = V_{th\text{-PBS}}$ (3600 s) $- V_{th\text{-PBS}}$ (0 s) = 3.93 V) without any changes in SS for PBS while V_{th} was shifted negatively ($\Delta V_{th\text{-NBS}} = V_{th\text{-NBS}}$ (0 s) $- V_{th\text{-NBS}}$ (3600 s) = 4.89 V) with the increase in SS for NBS; $V_{th\text{-PBS}}$ (3600 s) denotes V_{th} at $\tau_{st} = 3600$ s for PBS.

Table I. Summary of the important device parameters at two stress times of 0 and 3600 s for the unpassivated a-IGZO based TFTs under PBS and NBS.

Sample condition	Stress time (s)	V_{th} (V)	μ_{eff} (cm^2/Vs)	SS (V/dec)	On/off ratio
Unpassivated	0	−2.17	5.61	0.36	4.81×10^7
TFTs under PBS	3600	1.76	5.05	0.36	2.14×10^7
Unpassivated	0	−2.99	8.74	0.24	1.04×10^7
TFTs under NBS	3600	−7.88	7.98	0.54	1.69×10^7

However, no significant changes in the field-effect mobility and the on/off ratio of I_{DS} were observed for both bias stress cases. It has been reported[17] that the parallel shift in V_{th} without any change in SS during the stress time is attributed to simple charge trapping in the gate insulator and/or at the channel-insulator interface instead of the creation of defects within the channel materials. It has also been claimed[17, 27, 28] that the shift in V_{th} accompanying the change in SS comes from adsorption–desorption of oxygen and/or water molecules from ambient onto the exposed IGZO backsurface (which is called as ambient effect). Therefore, our results for the unpassivated a-IGZO-based TFTs indicate that the electron trapping model can by itself explain the PBS behavior, whereas the NBS behavior is associated with adsorption of water molecules from ambient onto the exposed IGZO backsurface. It is noteworthy mentioning that for NBS, the adsorption of water molecules induces the deep level and donor-like trap states within the energy band gap of the a-IGZO channel layer, resulting in the increase in SS and the negative shift in V_{th} without significant changes in the field-effect mobility. However, it was reported[17, 23] that in case of unpassivated a-IGZO TFTs with the plasma-damaged IGZO surface under PBS, the adsorption of oxygen on the IGZO surface creates acceptor-like trap states and contributes to the positive shift in V_{th} with the change in SS. This PBS result is different from our result because during our unpassivated TFT fabrication, the channel and source/drain electrodes were patterned by shadow mask instead of dry etching, indicating that our TFTs have the IGZO surface without a plasma-induced damage.

To explore the plausible mechanism behind the changes in reliability of a-IGZO TFTs, the changes in the SIMS depth profiles of oxygen (O), carbon (C), hydrogen (H), zinc (Zn), and silicon (Si) in SOG/IGZO/SiO_2/Si TFT structures were monitored. The SIMS depth profile of the TFTs passivated with SOG heat-treated at 100 °C indicated that the introduction of C and H from SOG into a-IGZO channel films occurred. This suggests that the a-IGZO layer of the sample passivated with SOG heat-treated at 100 °C has higher C and H concentration compared to the unpassivated sample. It is well-known that H can act as shallow-donor in ZnO[29] and IGZO.[15] It has also been reported that C has three defect forms such as C at Zn site (C_{Zn}; donor), C at oxygen vacancy (V_O) site (C_{Vo}; acceptor), and C_{Zn} bonded to two interstitial oxygen (O_i) ($C_{Zn} + 2O_i$; acceptor) and that among them, C_{Zn} has the lowest formation energy in the oxygen-poor condition.[15] Therefore, we believe that our IGZO films with the oxygen-poor property have dominant donor-like defects of C_{Zn}. Based on aforementioned argument, for the passivated samples with SOG heat-treated at 100 °C, the PBS and NBS instabilities are likely mitigated and deteriorated by the insertion of H and C donor-like defects from SOG into IGZO, respectively, compared to the unpassivated sample.

Figure 2 shows the SIMS depth profiles which exhibit the percentage variations in O, C, and H concentrations in TFT structures after heat treatments at temperatures in the range from 100 to 300 °C. The concentration changes are normalized with respect to the initial concentrations in the TFT structure treated with the temperature of 100 °C by using following Eq. (2):

$$\Delta I(\%) = \frac{I_T - I_{100\,^\circ\mathrm{C}}}{I_{100\,^\circ\mathrm{C}}} \times 100 \tag{2}$$

where I_T and $I_{100\ ^\circ\mathrm{C}}$ are the concentrations of O, C, and H at the temperature of T and 100 °C, respectively. In Eq. (2), the negative (positive) value of ΔI means the decrease (increase) of the concentration at T °C compared to the initial concentration at 100 °C. As shown in Figures 2(a and b), dominant amounts of C and H are noted to decrease in the IGZO channel layers for the passivated samples with SOG annealed at a higher temperature

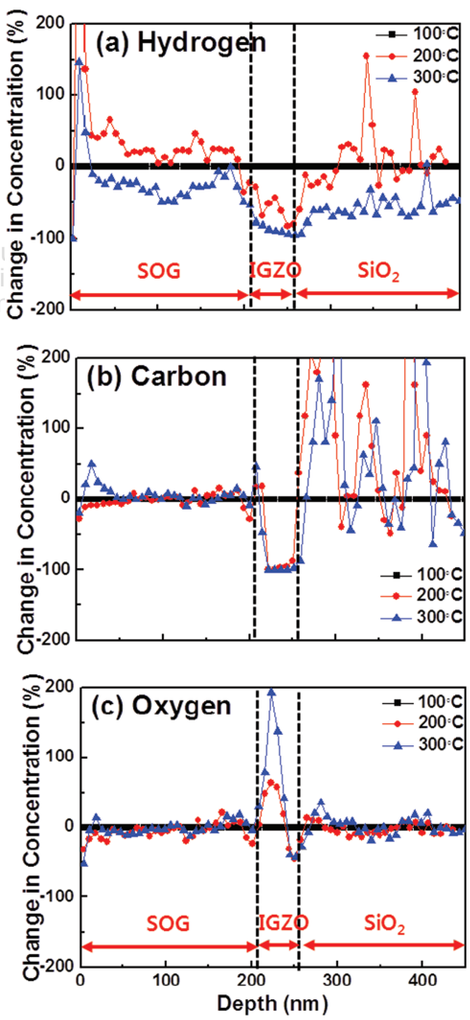

Figure 2. Percentage variations in (a) hydrogen (H), (b) carbon (C), and (c) oxygen (O) concentration in SOG/IGZO/SiO_2/Si TFT structures after heat treatments at temperatures in the range from 100 to 300 °C.

than 100 °C. This reduced C and H concentration apparently resulted in a decrease in the electron concentration in the IGZO films in the case of samples annealed at higher temperatures due to the reduction in C- and H-related donor defects. As plotted in Figure 2(c), however, for the change in the O depth profile, samples annealed at a higher temperature showed much larger increases in O concentration in the IGZO films compared to those annealed at 100 °C, indicating that a large amount of O diffused into the IGZO films during the treatment at higher temperatures of 200 and 300 °C. This causes an increase in the hole concentration in the films as a result of the formation of O_i acceptor defects. As a result, from Figure 2, we can predict that the PBS instability become worse by the increase of O_i acceptor defects in IGZO whereas the NBS instability is alleviated by the decrease of C- and H-related donor defects with increasing the anneal temperature for the samples passivated with SOG annealed at higher temperatures than 100 °C.

Table II summarizes the important device parameters at two τ_{st} values of 0 and 3600 s for the passivated a-IGZO TFTs with SOG annealed at three different temperatures of 100, 200, and 300 °C under PBS and NBS. These were obtained from the evolutions of the transfer curves as a function of τ_{st} for the passivated samples under PBS and NBS using Eq. (1). However, the device parameters of the samples with a 100 °C-annealed SOG under NBS were extracted up to 300 s instead of 3600 s due to the worst stabilities of the samples under NBS. In case of $\tau_{st} = 0$ s (before PBS or NBS is applied), as listed in Tables I and II, following changes are observed:

(1) large negative shift in V_{th} (−4.58 V) with the large increase in SS (0.77 V/dec.) was observed after the pristine devices were passivated with SOG annealed at 100 °C. This was attributed to the insertion of donor-like defects of C and H from SOG into IGZO and then

Table II. Summary of the important device parameters at two stress times of 0 and 3600 s for the a-IGZO TFTs passivated with SOG under PBS and NBS.

Anneal T of SOG (°C)/stress	Stress time (s)	V_{th} (V)	μ_{eff} (cm^2/Vs)	SS (V/dec)	On/off Ratio
100/PBS	0	−6.75	4.97	1.13	1.14×10^7
	3600	−5.58	3.96	1.08	9.63×10^6
200/PBS	0	0.99	3.12	0.89	5.50×10^6
	3600	3.10	2.93	0.83	2.94×10^6
300/PBS	0	−0.76	3.71	0.72	7.99×10^6
	3600	0.65	3.17	0.61	4.26×10^6
100/NBS	0	−10.08	4.23	0.80	1.01×10^6
	300[a]	−12.39	3.97	1.10	1.12×10^6
200/NBS	0	0.08	3.91	0.98	4.62×10^6
	3600	−0.92	3.56	0.77	6.13×10^6
300/NBS	0	0.05	3.12	0.80	4.86×10^6
	3600	−1.32	3.17	0.61	5.89×10^6

Note: [a]Used the data at 300 s instead of 3600 s due to the measurement limitation.

(2) large positive shift in V_{th} (7.74 V) without significant change in SS was observed for devices passivated with SOG annealed at 200 and 300 °C, which is associated with the reduction of C- and H-related donor defects and the increase of O_i acceptors in IGZO, as confirmed by Figure 2.

To clarify the possible mechanism behind the instability of a-IGZO TFTs during PBS and NBS, the changes in V_{th} and SS with different anneal temperatures of SOG for PBS and NBS were replotted using data listed in Tables I and II and they are shown in Figure 3. For the unpassivated samples under PBS and NBS, the V_{th} shift window ($V_{th\text{-}sw} = \Delta V_{th\text{-}PBS} + \Delta V_{th\text{-}NBS} = 8.82$ V), which is defined as the addition of V_{th} shift under PBS ($\Delta V_{th\text{-}PBS}$) and V_{th} shift under NBS ($\Delta V_{th\text{-}NBS}$), was very large. The SS shift window ($SS_{sw} = \Delta SS_{PBS} + \Delta SS_{NBS} = 0 + 0.3$) was also 0.3 V/dec; $\Delta SS_{PBS\,(NBS)}$ represents SS shift under PBS (NBS). These results confirmed that the stability of the unpassivated samples against PBS and NBS was poor. Therefore, we concluded that in our unpassivated IGZO TFTs, the PBS and NBS instabilities were attributed to the electron trapping at the channel-insulator interface and the adsorption of water molecules onto the channel backsurface, respectively. The large increase in $V_{th\text{-}sw}$ with huge increase in SS_{sw}, which is due mainly to NBS

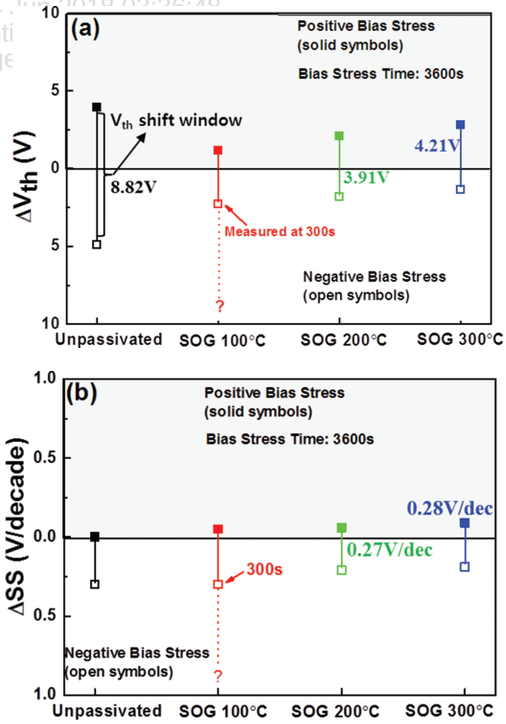

Figure 3. (a) V_{th} shift window ($V_{th\text{-}sw} = \Delta V_{th\text{-}PBS} + \Delta V_{th\text{-}NBS}$) and (b) SS shift window ($SS_{sw} = \Delta SS_{PBS} + \Delta SS_{NBS}$) as a function of anneal temperatures of SOG for PBS and NBS; $\Delta V_{th\text{-}PBS\,(NBS)}$ is V_{th} shift under PBS (NBS) and $\Delta SS_{PBS\,(NBS)}$ represents SS shift under PBS (NBS), respectively.

instability, was also observed for the passivated samples with a 100 °C-annealed SOG, confirming that the PBS instability was almost vanished by the annihilation of electron trapping and the NBS instability became much worse by the increase of electron density in IGZO because of the injection of H and C donor-like defects from SOG into IGZO after annealing SOG at 100 °C. Figure 3 also illustrated that with increasing the anneal temperature of SOG from 100 to 300 °C, the PBS stability was degraded and the NBS stability was improved, which are associated with the increase of O_i acceptor defects and the decrease of C- and H-related donor defects in IGZO, as evidenced by Figure 2. Among all samples prepared in this study, the passivated IGZO TFTs with a 200 °C-annealed SOG exhibited the best stability against PBS and NBS with $V_{th\text{-}sw} = 3.91$ V and $SS_{sw} = 0.27$ V/dec.

4. CONCLUSION

The stability characteristics against PBS and NBS of a-IGZO TFTs with new organic passivation layer of methyl-siloxane based SOG deposited by a sol–gel method were demonstrated. For the unpassivated TFTs, it was concluded that the electron trapping model can by itself explain the PBS behavior, whereas the NBS behavior is associated with adsorption of water molecules from ambient onto the exposed IGZO backsurface. In case of the passivated samples with SOG annealed at 100 °C in ambient air, compared to the unpassivated sample, the PBS instability was mitigated by the annihilation of electron trapping at the channel-insulator interface and the NBS instability became much worse by the increase of electron density in IGZO, which were due mainly to the insertion of H and C donor-like defects from SOG into IGZO. With increasing the anneal temperature of SOG from 100 to 300 °C, the PBS stability was degraded and the NBS stability was improved, which are related to the increase of O_i acceptor defects in IGZO and the decrease of C- and H-related donor defects. Among all samples prepared in this study, the passivated IGZO TFTs with a 200 °C-annealed SOG exhibited the best stability against PBS and NBS.

Acknowledgment: This research was supported by the Academic Research Fund of Hoseo University in 2015 (2015-0099).

References and Notes

1. K. Nomura, H. Ohta, K. Ueda, T. Kamiya, M. Hirano, and H. Hosono, *Science* 300, 1269 **(2003)**.
2. T. Kamiya and H. Hosono, *Int. J. Appl. Ceram. Tech.* 2, 285 **(2005)**.
3. K. Nomura, T. Kamiya, H. Ohta, T. Uruga, M. Hirano, and H. Hosono, *Phys. Rev. B* 75, 35212 **(2007)**.
4. T. Moriga, D. R. Kammler, and T. O. Mason, *J. Am. Ceram. Soc.* 82, 2705 **(1999)**.
5. M. Orita, H. Tanji, M. Mizuno, H. Adachi, and I. Tanaka, *Phys. Rev. B* 61, 1811 **(2000)**.
6. K. Abe, N. Kaji, H. Kumomi, K. Nomura, T. Kamiya, M. Hirano, and H. Hosono, *IEEE Trans. Electron Devices* 58, 3463 **(2011)**.
7. J. Jeong, J. Kim, G. J. Lee, and B.-D. Choi, *Appl. Phys. Lett.* 100, 023506 **(2012)**.
8. J. Jeong, G. J. Lee, J. Kim, S. M. Jeong, and E. J.-H. Kim, *J. Appl. Phys.* 114, 094502 **(2013)**.
9. M. Mativenga, S. An, S. Lee, J. Um, D. Geng, R. K. Mruthyunjaya, G. N. Heiler, and T. J. Tredwell, *IEEE Trans. Electron Devices* 61, 2106 **(2014)**.
10. S. P. Chang, Y. W. Song, S. G. Lee, S. Y. Lee, and B. K. Ju, *Appl. Phys. Lett.* 92, 192104 **(2008)**.
11. Y. Shimura, K. Nomura, H. Yanagi, T. Kamiya, M. Hirano, and H. Hosono, *Thin Solid Films* 516, 5899 **(2008)**.
12. H. Oh, S.-H. Ko Park, C.-S. Hwang, S. Yang, and M. K. Ryu, *Appl. Phys. Lett.* 99, 022105 **(2011)**.
13. W.-T. Chen, S.-Y. Lo, S.-C. Kao, H.-W. Zan, C.-C. Tsai, J.-H. Lin, C.-H. Fang, and C.-C. Lee, *IEEE Electron Dev. Lett.* 32, 1552 **(2011)**.
14. R. Zhan, C. Dong, P.-T. Liu, and H.-P. D. Shieh, *Microelectronics Reliability* 53, 1879 **(2013)**.
15. J. P. Bermundo, Y. Ishikawa, H. Yamazaki, T. Nonaka, and Y. Uraoka, *ECS J. Solid State Sci. and Technol.* 3, Q16 **(2014)**.
16. J. P. Bermundo, Y. Ishikawa, H. Yamazaki, T. Nonaka, M. N. Fujii, and Y. Uraoka, *Appl. Phys. Lett.* 107, 033504 **(2015)**.
17. J. K. Jeong, H. W. Yang, J. H. Jeong, Y.G. Mo, and H. D. Kim, *Appl. Phys. Lett.* 93, 123508 **(2008)**.
18. J. Wu, Y. Chen, D. Zhou, Z. Hu, H. Xie, and C. Dong, *Mater. Sci. Semicond. Process* 29, 277 **(2015)**.
19. J. Li, F. Zhou, H.-P. Lin, W.-Q. Zhu, J.-H. Zhang, X.-Y. Jiang, and Z.-L. Zhang, *Vaccum* 86, 1840 **(2012)**.
20. S.-Y. Huang, T.-C. Chang, M.-C. Chen, T.-C. Chen, F.-Y. Jian, Y.-C. Chen, H.-C. Huang, and D.-S. Gan, *Surface and Coatings Technology* 231, 117 **(2013)**.
21. D. Y. Yoo, E. Chong, D. H. Kim, B. K. Ju, and S. Y. Lee, *Thin Solid Films* 520, 3783 **(2012)**.
22. Z. Hu, D. Zhou, L. Xu, Q. Wu, H. Xie, and C. Dong, *Solid-State Electronics* 104, 39 **(2015)**.
23. M. Kim, J. H. Jeong, H. J. Lee, T. K. Ahn, H. S. Shin, J.-S. Park, J. K. Jeong, Y.-G. Mo, and H. D. Kim, *Appl. Phys. Lett.* 90, 212114 **(2007)**.
24. H. Xu, L. Lan, M. Xu, J. Zou, L. Wang, D. Wang, and J. Peng, *Appl. Phys. Lett.* 99, 253501 **(2011)**.
25. G.-W. Chang, T.-C. Chang, Y.-E. Syu, T.-M. Tsai, K.-C. Chang, C.-H. Tu, F.-Y. Jian, Y.-C. Hung, and Y.-H. Tai, *Thin Solid Films* 520, 1608 **(2011)**.
26. S.-H. Choi, J.-H. Jang, K. Jang-Joo, and M.-K. Han, *IEEE Electron Device Lett.* 33, 381 **(2012)**.
27. J.-S. Park, J. K. Jeong, H.-J. Chung, Y.-G. Mo, and H. D. Kim, *Appl. Phys. Lett.* 92, 072104 **(2008)**.
28. D. Kang, H. Lim, C. Kim, I. Song, J. Park, and Y. Park, *Appl. Phys. Lett.* 90, 192101 **(2007)**.
29. J. J. Dong, X. W. Zhang, J. B. You, P. F. Cai, Z. G. Yin, Q. An, X. B. Ma, P. Jin, Z. G. Wang, and P. K. Chu, *ACS Appl. Mater. Interf.* 2, 1780 **(2010)**.

Received: 14 March 2016. Accepted: 20 April 2016.